Golbabaie *et al.*
Sustainable Environment Research (2023) 33:28
https://doi.org/10.1186/s42834-023-00190-x

Sustainable Environment Research

RESEARCH

Open Access

Efficient degradation of various recalcitrant azo dyes in aqueous medium by immobilized *Origanum vulgare* peroxidase

Mahsa Golbabaie[1], Behzad Gharahchei[1], Fatemeh Mirazizi[1], Alireza Abbasi Baharanchi[1], Ali Khosronejad[1], Ali Asghar Karkhanie[1] and Kamahldin Haghbeen[1*]

Abstract

Hybrid xerogels, constructed from organic and inorganic silanes, have emerged as materials with versatile applications. They have shown promising potential for immobilization as their chemical structures encompass the mechanical, thermal, and structural stability of inorganic compounds in synergy with the functionality and flexibility of organic compounds. Incorporating a magnetic core and preparation at the nanoscale multiply their attraction for enzyme immobilization. To evaluate how efficiently this technology works for the immobilization of a plant peroxidase, a novel peroxidase (POX_{ov}) from a famous medicinal herb, *Origanum vulgare*, was immobilized on magnetic nanoparticles of a hybrid xerogel obtained from tetraethyl orthosilicate and (3-aminopropyl)triethoxysilane. Immobilization boosted the physicochemical properties of the enzyme so that the immobilized POX_{ov} ($I.POX_{ov}$) could tolerate lower pHs and higher temperatures. It oxidized all types of the examined phenolic, catecholic, guaiacolic, and aniline diazo dyes, while the free POX_{ov} ($F.POX_{ov}$) failed to oxidize the last group. These improvements also made $I.POX_{ov}$ capable of oxidizing the recalcitrant azo dyes carrying electron-withdrawing groups much faster than $F.POX_{ov}$. $I.POX_{ov}$ was employed in 7 successive cycles of oxidation of both phenolic and guaiacolic dyes with an average efficiency of 69%. The efficacy of the immobilization method and I.POXov competency for the enzymatic remediation of polluted water resources have been quantitatively demonstrated.

Keywords Aniline azo dyes, Enzymatic bioremediation, Magnetized nanoparticles, Polluted water resources

1 Introduction

Oxidoreductases are effective enzymes for the biotransformation, oxidation, and decomposition of aromatic compounds [1]. In a comparative study, it was shown that peroxidase (POX) had a superior ability for the removal of diazo dyes as compared with tyrosinase (EC 1.14.18.1) and laccase (EC 1.10.3.2) [2]. POXs with versatile physicochemical qualities, broad spectra of substrates, and high operational stability can be extracted from safe sources such as edible plants [3]. Consequently, immobilization of such enzymes is a hot topic of environmental science and engineering.

Immobilization allows easy separation of the enzyme from the reaction medium and permits several successive uses of the immobilized enzyme. It might also improve the physicochemical properties of the immobilized enzyme [4]. No doubt that enzyme immobilization needs a suitable carrier. Due to the large ratio of surface to volume, possible surface modifications, and easy preparations, iron oxide nanoparticles have emerged as the cornerstone for developing various magnetic carriers for molecules such as enzymes [5]. Considering the

*Correspondence:
Kamahldin Haghbeen
Kamahl@nigeb.ac.ir
[1] Department of Agricultural Biotechnology, National Institute for Genetic Engineering and Biotechnology, Tehran 1497716316, Iran

advantages of the sol-gel process, magnetized xerogels with modified surfaces have come to attention as non-toxic matrices for immobilization purposes. Nonetheless, the challenges of POX immobilization on this type of support have received little attention while there is a growing demand for the applications of immobilized POXs in the combats against organic pollutants, especially diazo dyes.

Diazo dyes form a large group of synthetic organic dyes, embracing 50% of the total dyes produced worldwide [6]. Many of these dyes are discharged daily into the effluents of different industries threatening surface and groundwater sources [7, 8]. In addition to their adverse impact on the chemical oxygen demand to biological oxygen demand ratio of water, it is known that they are potentially carcinogenic and mutagenic [6]. Therefore, the treatment of the wastewater of dyes manufacturers and consuming units and the removal of these dyes from aqueous mediums have been the focus of environmental research in the past four decades [7].

Several physical, chemical, and physicochemical methods, such as membrane filtration, nanofiltration, reverse osmosis, precipitation, flotation, ion exchange, activated sludge, photolysis, electrolysis, and various advanced oxidation processes have been studied for the decontamination of polluted waters. The advantages and disadvantages of these methods have been comprehensively reviewed [7, 8]. These studies indicate problems such as the formation of large volumes of sludge, high-energy consumption, and high expenses of the processes have led researchers to pay attention to biotechnology-based methods. As a result, enzymatic remediation of the contaminated water resources, alone and in combination with other methods, has received particular attention. Enzymatic-based methods are eco-friendly and are run under milder conditions that reduce costs and decrease sludge production with no or less toxic byproduct formation [9, 10]. In pursuit of this trend, a novel POX from the cell culture of *Origanum vulgare* (POX_{ov}) [11] was immobilized on a biocompatible magnetized hybrid xerogel (MHyX). Then, a comparative study was conducted to examine decomposition of different diazo dyes in an aqueous medium by the free ($F.POX_{ov}$) and immobilized *O. vulgare* POX ($I.POX_{ov}$). The details of the experiments and the results are presented and discussed in terms of feasibility and efficacy.

2 Materials and methods

2.1 Materials and instruments

All the required chemicals and solvents were taken from the authentic samples. Diazo compounds (Fig. 1) were synthesized and purified according to the literature [12]. The stock solution concentration of each dye was 1 mg per 2 mL of methanol. POX_{ov} was prepared as described in the literature [11]. GASA (E)-4-[(4-hydroxy-3-methoxyphenyl)diazenyl]benzenesulfonic acid (III_d, Fig. 1) with an extinction coefficient of ($\varepsilon_{375} = 15{,}330\ cm^{-1}\ M^{-1}$ extracted from Fig. S1a in the Supplementary Materials) was used as the organic substrate in routine enzyme assays [13]. The bovine serum albumin (BSA) standard curve was obtained to measure the desired solutions' protein content (Fig. S1b). Spectrophotometric studies were conducted using a UV-Vis Specord 50 + spectrophotometer (Analytik Jena-Germany). Fourier-transform infrared spectroscopy (FTIR) spectra were recorded by a Bruker Tensor 27 FT-IR spectrophotometer using the conventional KBr disks of the samples. Scanning Electron Microscopy (SEM) images were obtained by VEGA3 TESCAN and MIRA3 TESCAN.

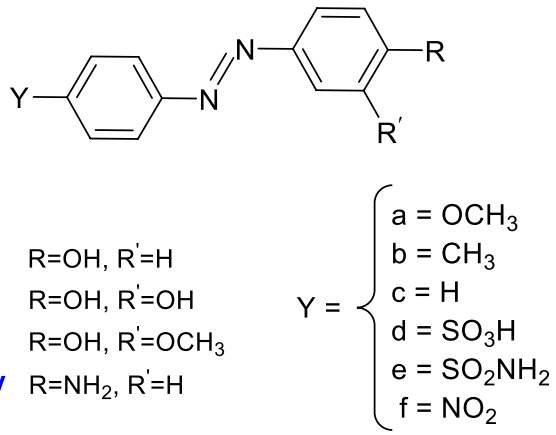

Fig. 1 Chemical structure of the examined diazo dyes used in this study

2.2 Synthesis of iron oxide nanoparticles

Several methods have been introduced for the bare and coated magnetic nanoparticles (MNP) preparation that result in particles of different sizes, crystallinity, and magnetic properties [14, 15]. In this work, with some modifications, an established method known as co-precipitation was employed under hydrothermal conditions to obtain MNP. Choosing the stoichiometric ratio in Fe_3O_4 synthesis from $Fe(OH)_2$ and FeOOH for the precursors ($Fe^{II}/Fe^{III} = 0.5$) and applying a mild heating, a one-pot reaction was run in the absence of any oxidant and co-solvent to produce MNP with average sizes between 2 and 40 nm [15] and the characteristic black color of magnetite (Fig. 2a). Thus, $FeCl_2.4H_2O$ (2 g) and $FeCl_3.6H_2O$ (5.4 g) were mixed at a molar ratio of 1:2 in double distilled water (100 mL). The mixture was degassed by N_2. Then, ammonia (25%, 25 mL) was added dropwise to the mixture on a stirrer for 30 min under

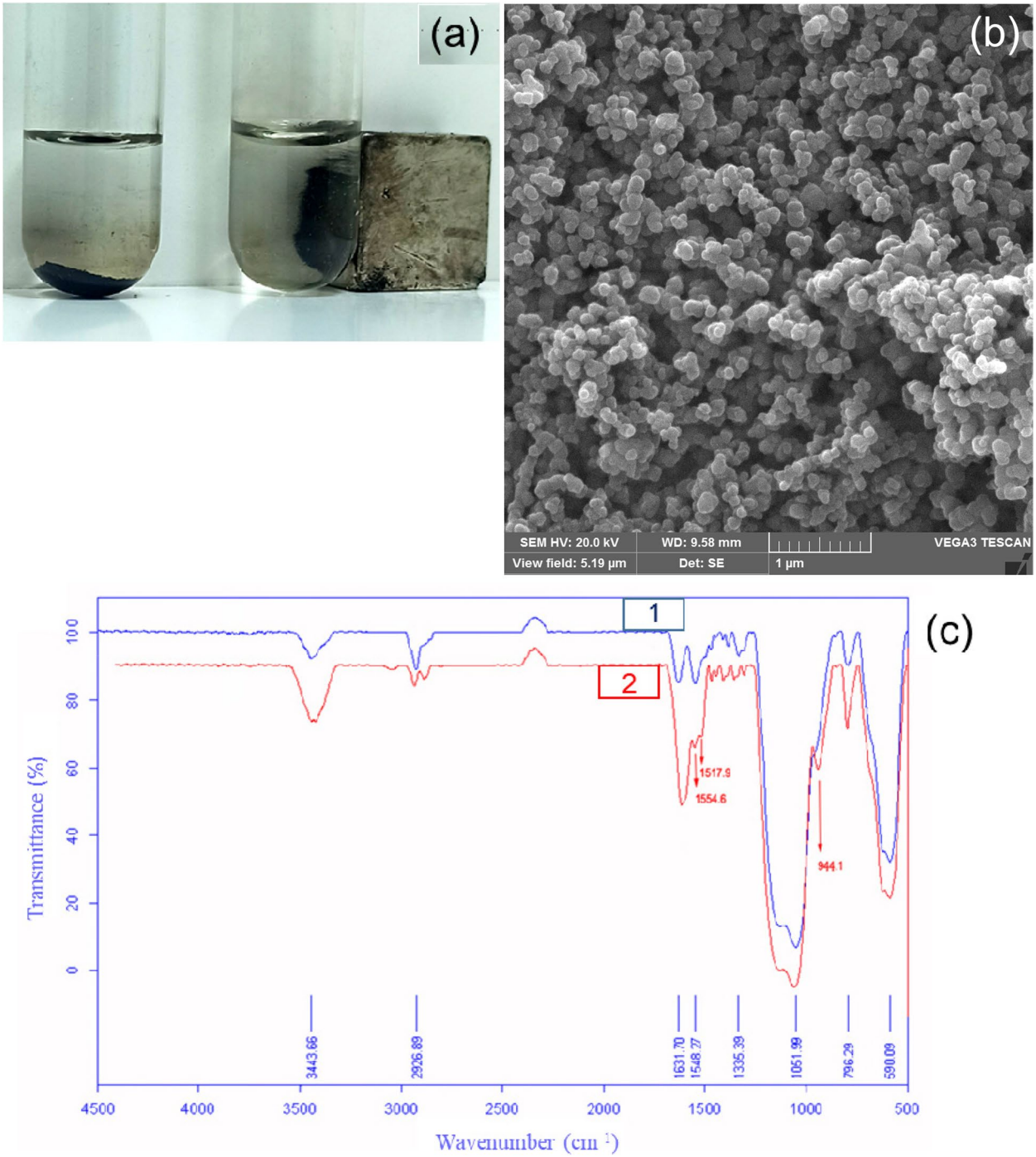

Fig. 2 **a** Reaction of the prepared MHyX to a magnetic bar. **b** The SEM of the prepared MHyX. **c** Overlaid FTIR spectra of (1) MHyX and (2) MHyX-CyC

the N_2 atmosphere. Finally, it was heated in a bain marie (80 °C) for 30 min [16]. The resulting nanoparticles were separated from the mixture by a magnet, washed three times with deionized water, and dried at ambient temperature. It was shown that shortening the heating time decreases the particle average sizes < 20 nm [16].

2.3 Magnetic hybrid xerogel (MHyX) preparation

MNP was coated by the hybrid xerogel of tetraethyl orthosilicate (TEOS) and (3-aminopropyl)triethoxysilane (APTES). Xerogels are prepared through a facile, cost-effective, and relatively fast process that is implemented under ambient conditions [17]. Although the

classical preparation of xerogels from tetra-alkoxysilanes results in mesoporous brittle materials with hydrophilic surfaces [18], the process can be readily modified to produce more robust nanoparticles with the desired physicochemical properties [17, 19]. Adding an ormosil such as APTES to TEOS creates a hybrid xerogel with modified hydrophobicity and improved mechanical strength [17]. APTES also provides the final product with amino nucleophilic groups [20]. Finally, seeding the sol-gel formation with iron oxide nanoparticles results in magnetized nano-hybrid-xerogel (MHyX) particles that can be easily separated from the reaction medium by a magnet bar (Fig. 2a).

MHyX was prepared by hydrolysis of a mixture of TEOS and APTES (4:1 molar ratio) by the sol-gel method in the presence of iron oxide nanoparticles. Therefore, Fe_3O_4 nanoparticles (400 mg) in ethanol (96%, 100 mL) were sonicated for 10 min for the nanoparticle dispersion. Then, TEOS (1374 µL) and APTES (274 µL) were first mixed then added to the sonicated Fe_3O_4 solution while double distilled water (20 mL) was added to the mixture. The resulting mixture was sonicated for another 30 min. Next, when the sonicator was still on, ammonia (25%, 50 µL) was added to the mixture, and sonication continued for 5 min. The resulting suspension was shaken (80 rpm) for 3 h at room temperature before centrifugation (10 min, 4 °C, 8000 rpm). Collected particles were dried at ambient temperature overnight. To obtain MHyX with uniform sizes, the particles were passed through a sieve (0.037 mm, 400 mesh).

2.4 Immobilization of POX_{ov} onto MHyX

The cross-linker, cyanuric chloride (CyC, 125.5 mg), was dissolved in acetone (40 mL) containing MHyX particles (313 mg). The mixture was gently shaken for 2 h at 4 °C. Finally, the particles were washed three times with acetone and three times with double distilled water. To react all the free amino groups on the MHyX surface with the cross-linker, 2 mg of CyC per 5 mg of MHyX was applied.

To immobilize the enzyme, the particles of the previous step (300 mg) were added to 2 mL of the POX_{ov} solution (0.13 mg mL^{-1}). The mixture was shaken (80 rpm) at ambient temperature for 8 h. Finally, a magnet separated the particles from the mixture and washed them three times with deionized water. The residue was dried at room temperature for 1–2 d, then stored in an amber glass at 4 °C.

2.5 Kinetics of free and immobilized POX_{ov} activities

The catalytic activities of $F.POX_{ov}$ and $I.POX_{ov}$ were assayed spectrophotometrically through the decrease in the optical density of GASA at 375 nm [13]. All the enzymatic reactions were carried out at 20 ± 2 °C in a conventional quartz cell containing 3 mL of the reaction mixture. Each reaction mixture had GASA (65 µM), H_2O_2 (7 mM), and an appropriate amount of $F.POX_{ov}$ (2 µL per mL of the reaction mixture) or $I.POX_{ov}$ (30 mg per mL of the reaction mixture). The enzymatic reactions of $F.POX_{ov}$ and $I.POX_{ov}$ were carried out in phosphate-buffered saline (PBS, 100 mM) at pH 6 and 5, respectively. At the end of $I.POX_{ov}$ reactions, the particles were separated from the reaction mixture by a magnet, and the solution was passed through a cotton swab to remove any suspended particles. All the experiments were performed in three replications. Statistical analysis was performed using the Microsoft Excel software. The $F.POX_{ov}$ reactions were followed for 10 min but the $I.POX_{ov}$ reactions were measured at 3, 6, and 12 min intervals.

2.6 Removal of diazo dyes at the optimal pH and temperature of $F.POX_{ov}$ and $I.POX_{ov}$

The optimal pH and temperature of $F.POX_{ov}$ and $I.POX_{ov}$ activities were studied in the ranges of 3–8 and 20–80 °C, respectively, using the mentioned assay method. Then, the reactions of $F.POX_{ov}$ with various azo derivatives of phenol, catechol, guaiacol, and aniline (Fig. 1) were investigated spectrophotometrically at pH 6 and 20 ± 2 °C [2]. Finally, the efficacy of $I.POX_{ov}$ and $F.POX_{ov}$ for removing the selected azo dyes from the aqueous solution was examined in PBS (0.05 M) at the optimal pHs and 20 ± 2 °C. The oxidation rates were calculated from the decrease of the optical density of each dye at its λ_{max} per minute.

3 Results and discussion

3.1 Immobilization matrix

SEM image of the MHyX shows that the nanoparticles formed and agglomerated almost uniformed spherical-shape particles with an average diameter of 88 nm (Fig. 2b). It was shown that there was an inverse relationship between the size of the matrix particles and the enzyme uptake. But, particles smaller than 75 nm were prone to aggregation [21]. On the other hand, the larger particles tended to increase the interactions between the surfaces (the particle with the protein), extending the adsorption that could cause the unfolding of the protein skeleton [22]. The optimal size for immobilizing tyrosinase on nanoparticles was 75 to 150 nm [21].

The FTIR spectrum of the MHyX (Fig. 2c) exhibits the characteristic broad band of xerogels at 1051 cm^{-1} attributed to the stretching of Si-O-Si bonds [23]. It also shows a shoulder at 944 cm^{-1}, and a strong band at 590 cm^{-1} pertains to the stretching and rocking vibrations of the Si-OH bond, respectively. The weak band at 3443 cm^{-1} with a broad shoulder at smaller wave numbers (about 3300 cm^{-1}) are due to the stretching vibration of O-H

and N-H bonds indicating the presence of some free hydroxyl and amino groups on the surface of the MHyX. The band at 2926 cm^{-1} confirms the presence of the propyl C-H bonds. The weak transmittance band at 1548 also indicates the presence of the amino group [23].

3.2 Immobilization of POX_{ov} on MHyX

3.2.1 Activated MHyX

The efficacy of immobilization partly depends on the quality of the cross-linker that is responsible for attaching the macromolecule to the surface of the matrix. Glutaraldehyde is widely used for this purpose but, in addition to intermolecular cross-linking, it can participate in intramolecular reactions such as the ring closure reaction with nucleophilic residues on the surface of the matrix that originates from the high degree of freedom of its C5-chain. Furthermore, the reactivity of the aldehyde functional group facilitates the glutaraldehyde participation in polymerization through condensation reactions [24]. In contrast, the planar structure of CyC has a limited degree of freedom [25], and the displacement of the chloride groups can be controlled effectively by controlling the temperature of the coupling reaction [26]. It was demonstrated that CyC preferentially reacted with the amino group when both amino and hydroxyl groups were present [27]. Therefore, to activate MHyX, CyC was used as the cross-linker. By keeping the temperature below 4 °C, it was possible to successfully substitute one of the CyC chlorides in the reaction with MHyX in 2 h. Although the transmittance bands of MHyX cover the characteristic vibrational bands of the triazine ring of CyC (1449.2, 1562.5 cm^{-1} in-plane, and 816.3 cm^{-1} out-of-plane ring vibrations [28]), the presence of CyC on the MHyX is recognized from Fig. 2c, where the shoulder of the broadband at 3300 cm^{-1} along with the bending vibration of N-H about 1540 cm^{-1} has been weakened, while the band close to 1630 cm^{-1} has been boosted because of the presence of C=N.

3.2.2 POX_{ov} immobilization

After binding CyC to the surface of matrix, the substituted amino group deactivates the remaining two chlorides of CyC toward nucleophilic substitution so that the subsequent substitutions occur at higher temperatures [29]. Consequently, to immobilize POX_{ov}, the coupling reaction of the enzyme with the MHyX-CyC was run at room temperature [29]. Using CyC as the cross-linker, Banjanac et al. successfully immobilized lipase on a modified fumed nano-silica surface at room temperature [30]. The coupling reaction of our research was examined in deionized water, double-distilled water, and PBS (pH 7). The results favored deionized water (pH 4.5) (Fig. S2a). This condition was close to that used for the co-immobilization of horseradish peroxidase (HRP) and tyrosinase on a hybrid xerogel matrix [31]. It is clear that the free amino residues of a protein are not protonated at pH > 4, so they can take part in coupling reaction with CyC, but at pH > 7, the rate of the hydrolysis of CyC chlorides increases. Banjanac et al. carried out the coupling reaction of lipase at pH 7 without presenting any optimization data [30]. The examinations also proved that the coupling reaction could reach completion in 8 h. $I.POX_{ov}$, obtained from the 8 h coupling reaction, almost flattened the substrate peak after elapsing the assay time (Fig. S2b) indicating about 90% removal efficiency (Fig. S2c).

The FTIR spectra of an immobilized protein on a surface exhibit 3 bands associated with the amide I (C=O stretching mode), amide II (NH deformation), and amide III (C-N stretching and NH bending motions) vibrational modes. However, the band of amide I (around 1630 cm^{-1}) is usually taken into account as a diagnostic one, and the other two (between 1510 and 1560 and 1200–1300 cm^{-1}, respectively) are poorly diagnostic due to the overlapping with strong C=N, C-O, and C-N stretching bands [32]. Both bands, above 1500 and 1600 cm^{-1}, have been boosted in the FTIR spectrum of $I.POX_{ov}$ (Fig. 3a) assumingly due to the presence of CyC and the attached enzyme while the stretching band of N-H (above 3300 cm^{-1}) has faded. Finally, the SEM image (Fig. 3b) confirms the effective binding of POX_{ov} to MHyX-CyC.

3.3 Operating parameters of $I.POX_{ov}$

Figure 4a reveals that immobilization of POX_{ov} on the MHyX shifted the optimal activity of the enzyme toward lower pH(s). In contrast to $F.POX_{ov}$, which suffered a colossal activity loss at pHs < 4, $I.POX_{ov}$ tolerated the harsh conditions of the acidic medium as low as pH 3 while maintained > 65% of its activity in the pH range of 6 to 7. This advantage allows enzymatic treatment of the acidic wastewater, where the low pH stress hampers microbial bioremediation [33]. Immobilization also increased the optimal temperature of activity of POX_{ov} from 30 to 40 °C (Fig. 4b). This indicates higher structural stability of $I.POX_{ov}$ over $F.POX_{ov}$. Many plant POXs show a sharp decrease in activity because of either pH or temperature changes. There are 4 disulfide bonds, two Ca^{2+} ions, and one ionic bridge that play critical roles in stabilizing the structures of plant POXs [34]. Consequently, there are thresholds for the disulfide bonds to cleave, Ca^{2+} ions to jump out, and the bridge salt to breakdown. When the temperature rises to the threshold, the 3D structure collapses.

The powder of $I.POX_{ov}$ could maintain > 55% of its activity after 3 months of storage at 4 °C under the normal atmosphere (Fig. 4c). Functional stability examination showed that $I.POX_{ov}$ could maintain about 18% of

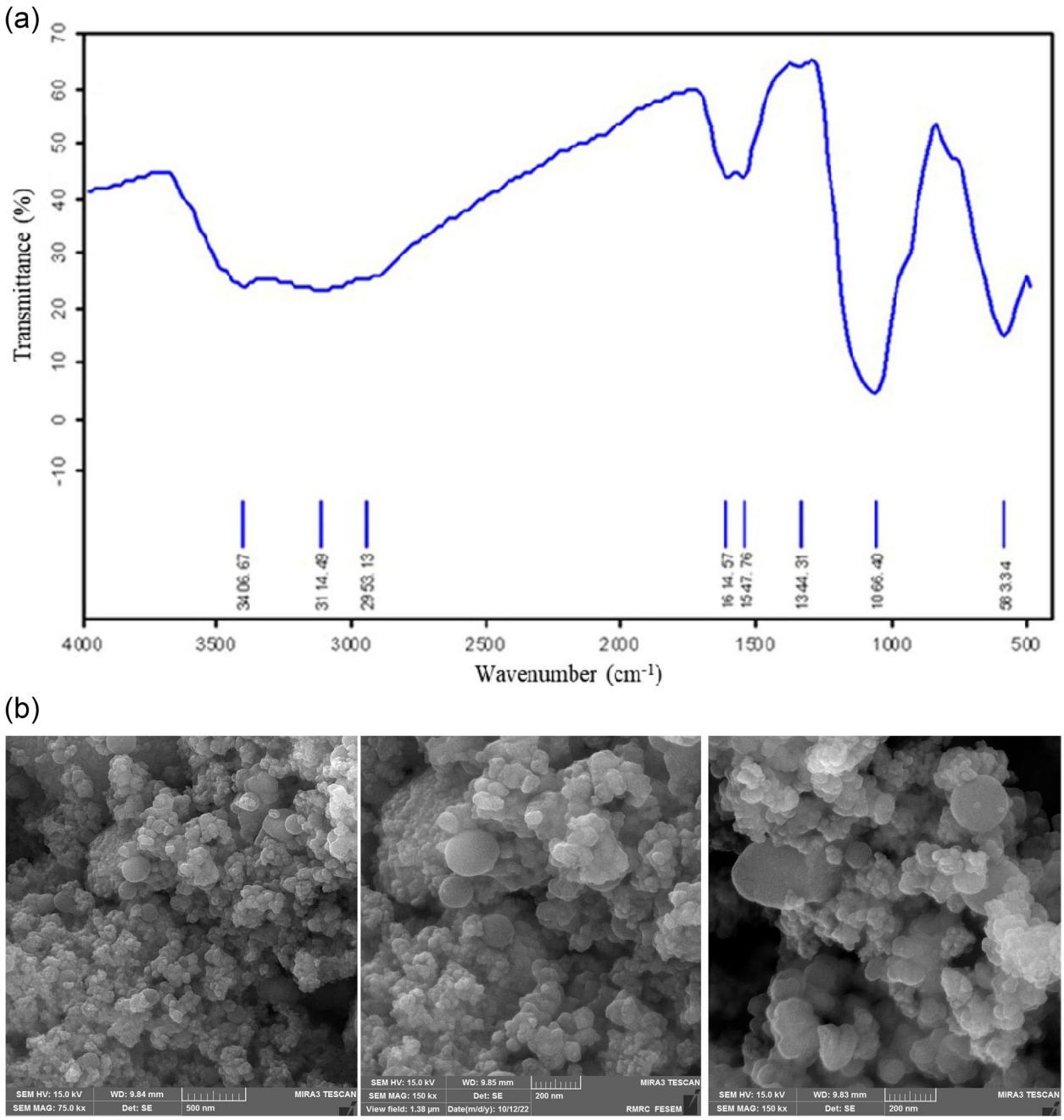

Fig. 3 **a** FTIR spectrum and (**b**) the SEM image of I.POX$_{ov}$ on MHyX-CyC

its initial activity after 7 successive cycles of reactions with an average efficiency of 69% (Fig. 4d). These results indicate favorable interactions between the magnetized matrix and the structural elements of the enzyme that support the functional stability of I.POX$_{ov}$.

Using glutaraldehyde as a cross-linker, immobilization of a peroxidase obtained from the skin peels of Mexican turnip (Jicama) on the nanocomposite of carbon nanotubes/polyvinyl alcohol did not change the optimal pH and temperature of the immobilized enzyme but it increased the tolerance of the enzyme against the changes in temperature and pH. The immobilized peroxidase could also maintain 81% of its initial activity after 5 weeks of storage at 4 °C [35]. Covalent immobilization of HRP on polyacrylamide cryogel, functionalized by 1-Ethyl-3-(3-dimethylaminopropyl)

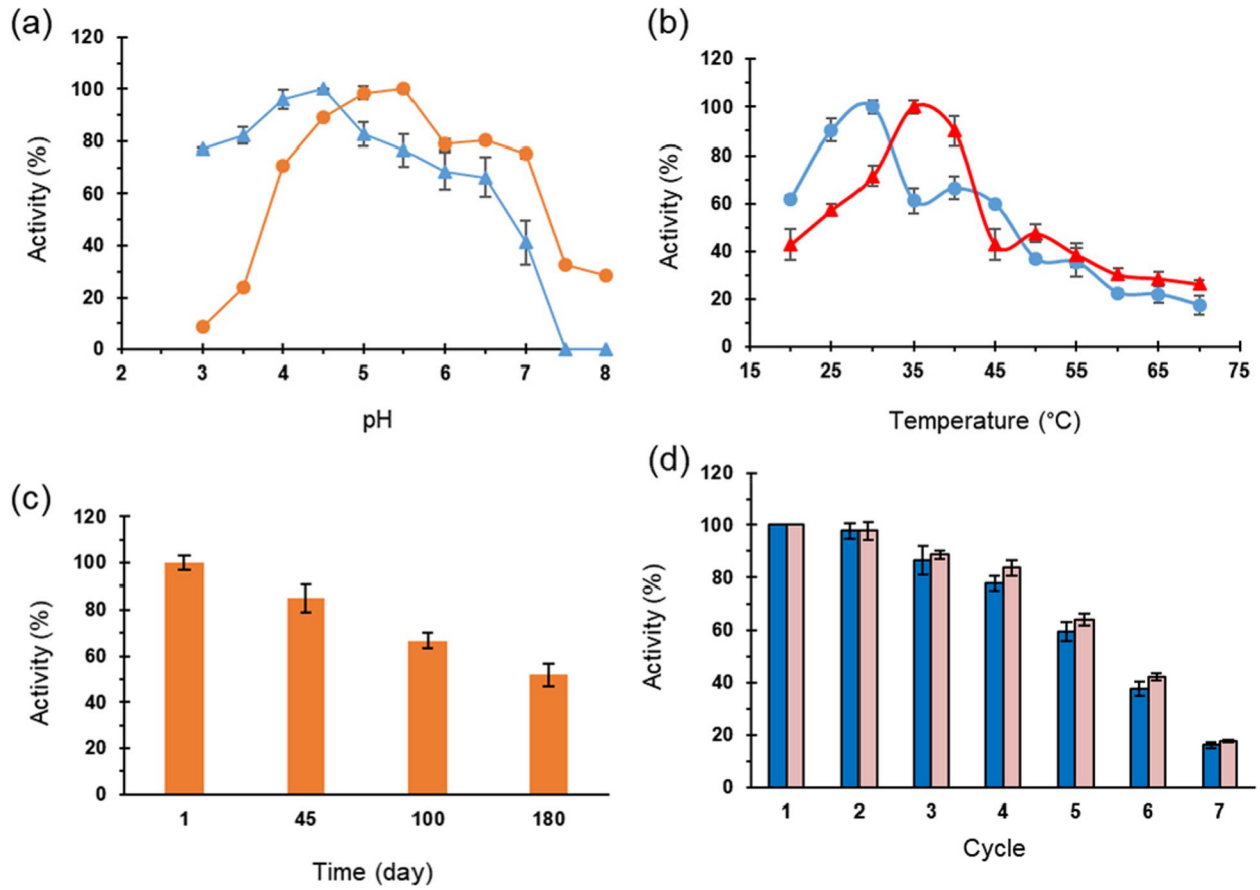

Fig. 4 Comparative optimal (**a**) pH(s) and (**b**) temperatures of I.POX$_{ov}$ (▲) and F.POX$_{ov}$ (●). The residual activity of I.POX$_{ov}$ (**c**) during storage at 4 °C, and (**d**) after successive oxidation of $\mathbf{I_a}$ (dark column) and $\mathbf{III_d}$ (light column). See the experimental section for the corresponding details

carbodiimide/N-hydroxysuccinimide, resulted in no changes in the optimal temperature of the enzyme. At the same time, it caused a little alkaline shift in the optimal pH of activity, and the immobilized peroxidase could maintain 68% of its initial activity after ten cycles of guaiacol oxidation [36]. It is worth mentioning that, in contrast to this article, the total time of each cycle was not mentioned in the assay methods, and the immobilized peroxidases were assayed in the presence of only one type of substrate [35, 36].

3.4 Substrate spectrum of I.POX$_{ov}$

F.POX$_{ov}$ could oxidize all the examined phenolic, guaiacolic, catecholic, and aniline diazo dyes. However, the oxidation rate of the last group was very slow (Fig. 5a). The oxidation reactions of F.POX$_{ov}$ was also sensitive to the nature of the substitutions on the structure of the dyes. As expected, dyes carrying electron-withdrawing groups were oxidized at lower paces (Fig. 5b). Interestingly, I.POX$_{ov}$ bypassed this limitation and oxidized aniline dyes at a comparable rate as the other types of diazo dyes. For instance, the instantaneous rate of $\mathbf{IV_b}$ oxidation (dA min^{-1} = 0.025) was close to the oxidation rate of $\mathbf{II_c}$, dA min^{-1} = 0.028 (Fig. 5c and d). The oxidation reactions by I.POX$_{ov}$ was also sensitive to the nature of the substituents but in a different way. I.POX$_{ov}$ unexpectedly accelerated the oxidation of the dyes carrying electron-withdrawing groups. Comparing the data presented in Fig. S3 reveals that the oxidation rates of $\mathbf{IV_c}$ and $\mathbf{IV_b}$ were boosted 7.1 and 4.2 times, respectively, while the reactions of $\mathbf{IV_f}$ and $\mathbf{IV_e}$ were increased about 100 times. Although uneven effects of the various substituents on the rates of radical reactions have been discussed in the literature [37], an explanation of this phenomenon needs more research because the magnetic field effect on electron transfer should also be taken into account.

3.5 POX$_{ov}$ immobilization efficacy

In addition to the typical absorption peaks of proteins at about 235 and 280 nm, the spectrophotometric spectrum of a plant POX shows the absorption band of heme at about 403 nm [34]. Accordingly, despite the interference

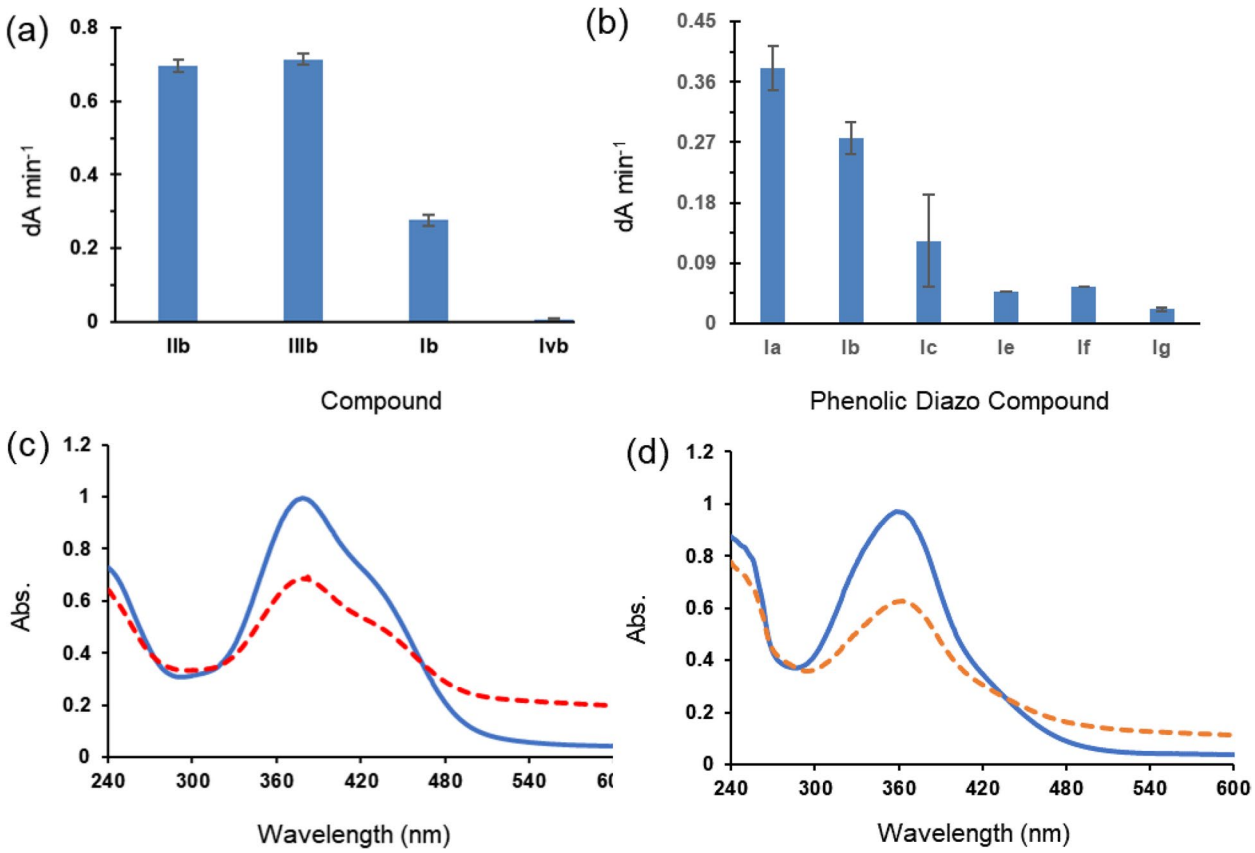

Fig. 5 Comparative instantaneous rates of oxidation of (**a**) different types of azo dyes and (**b**) different derivatives of phenolic diazo dyes by I.POX$_{ov}$. Overlaid spectra of the start and the end of oxidation of (**c**) **IV$_b$** and (d) **II$_c$** by I.POX$_{ov}$. All these reactions were carried out under identical conditions. Instantaneous rates obtained from the steady-state phases of the corresponding velocity graphs. See the experimental Sect. 2.6 for the details

of the residual nanoparticles at the 280 nm region, the efficiency of the coupling reaction of MHyX-CyC with F.POX$_{ov}$ could be measured reliably through the decrease of the heme absorbance (Fig. 6). The turbidity of the enzyme solution after the immobilization reaction caused a little background at 403 nm after the immobilization reaction (dash-line in Fig. 6). Nonetheless, this absorbance was ascribed to the possible residual of the uncoupled POX$_{ov}$. Given this fact, it is concluded that the enzyme uptake by the nanoparticles was at least 86%

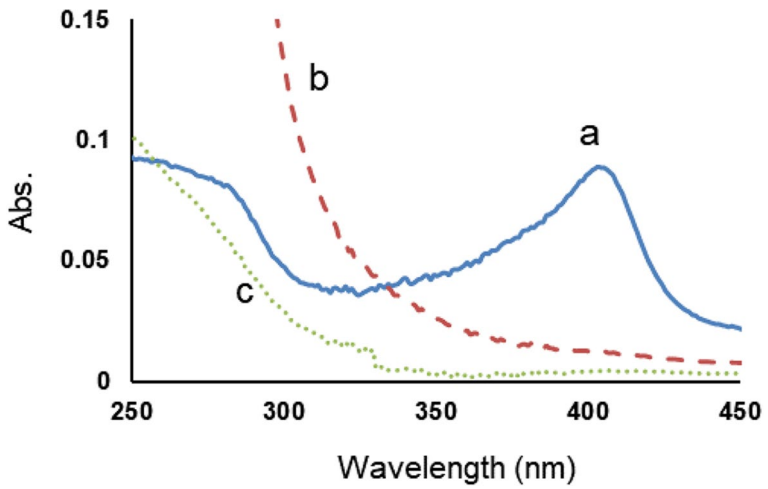

Fig. 6 UV-visible spectra of F.POX$_{ov}$ before (**a**), after (**b**) coupling reaction with MHyX-CyC and the wash solution of I.POX$_{ov}$ (**c**)

Table 1 The efficacy of POX_{ov} immobilization on activated MHyX

Solution	V (mL)	Abs. 280 nm	Abs. 403 nm	Rate dA min^{-1}	Unit of Activity[b] µM min^{-1}	Total Units of Activity µM min^{-1}
POX_{ov} (B.I.)	2	0.0813	0.089	0.108	7.05	7050
POX_{ov} (A.I.)	2	0.318	0.012	0.014	0.91	910
Wash	6	0.059	0.004	0.026	1.70	1020
I.POX_{ov}	30[a]			0.113	7.37	737[c]
Primary Uptake (%)	86[d]					
Washed Enzyme (%)	14[d]					
Effective load (%)	73					
Activity Recovery (%)	14[e]					

[a] 15 mg per mL, [b]based on the extinction coefficient of $\mathbf{III_d}$ at 375 nm pH 5 (15,330 cm^{-1} M^{-1}), [c]total amount of I.POX_{ov} = 300 mg, [d]based on absorbance at 403 nm, [e]based on total units of activity

Total Protein: 0.258 mg specific activity = 27315.5 (see the supplementary materials for the calculations)

successful. Table 1 also suggests that 14% of F.POX_{ov} was non-covalently bonded to the nanoparticles since it was found in the wash solution. Therefore, the effective load of enzyme onto the magnetic nanoparticle was 73%.

Examination of the enzyme activity revealed that I.POX_{ov} showed only 14% activity of the covalently-bond enzyme (Table 1). This means that about 85% of the immobilized POX_{ov} either lost its activity or was not accessible for the substrate. But, in contrast to F.POX_{ov}, it was possible to use I.POX_{ov} in 6 more successive cycles of reactions with an average efficiency of 64% (Fig. 4d). This makes 3567 units of activity equal to 51% of the total activity of the original F.POX_{ov} solution (7050 µM min^{-1}, (see the supplementary materials for the calculations of Table 1). A similar method was used to immobilize lipase, resulting in a higher recovery of the initial activity [38, 39]. Although the preparation methods of the matrices are not identical [38, 39], this difference in the outputs could be attributed to the different surface charges of these two enzymes and the existence of sensitive structural elements such as the heme cofactor and the disulfide bridges in plant POXs [34].

4 Conclusion

Considering the increasing applications of plant POXs for environmental purposes, such as enzymatic remediation of water resources, and the lack of data about the immobilization of such enzymes on magnetized xerogel as a safe, robust, and cost-effective carrier, the immobilization of POX_{ov} on the designed MHyX was demonstrated in a comparative and quatitative way. Immobilization boosted the physicochemical properties of POX_{ov} and made it capable of oxidizing the recalcitrant azo dyes carrying electron-withdrawing groups at an accelerated rate while F.POX_{ov} failed or was too slow. The qualifications of I.POX_{ov} allows its facile employment in the remediation of polluted water resources with variable pHs and the fabrication of various biosensors. The combination of the attractive physicochemical properties of POX_{ov} as well as the eco-friendly nature and facile preparation of MHyX support the large-scale development of this technology for enzymatic remediation of water resources.

Supplementary Information

The online version contains supplementary material available at https://doi.org/10.1186/s42834-023-00190-x.

Additional file 1. All data generated or analyzed during this study are included within the submitted manuscript and the Supplementary Materials. Additional files include Fig. S1. Standard curves of GASA extinction coefficient and Abs. at 280 nm vs. concentration of pure BSA. Fig. S2 The results of the coupling reaction of MHyX with CyC. Fig. S3. Spectrophotometric following the reactions of aniline diazo dyes with F.POX_{ov} and I.POX_{ov}.

Acknowledgements
The authors thank Mr. Javad Marefatjoo for his invaluable help in the preparation of pure enzyme.

Authors' contributions
M. Golbabaei, B. Gharachei, F. Mirazizi, A. Khosronejad, and A.A. Baharanchi: provided the data of different steps and software. A.A. Karkhanie: Methodology, Validation, Resources. K. Haghbeen: Conceptualization, Methodology, Resources, Supervision, Funding Acquisition. All authors participated in the preparation and reviewing of the manuscript.

Funding
Funding was provided by National Institute of Genetic Engineering and Biotechnology (Project 730).

Availability of data and materials
Supplementary material related to this article can be found in the online version at doi:

Declarations

Competing interests
The authors declare that they have no known competing financial interests or personal relationships that could have appeared to influence the work reported in this paper.

Received: 10 May 2023 Accepted: 4 September 2023
Published online: 12 September 2023

References

1. Jun LY, Yon LS, Mubarak NM, Bing CH, Pan S, Danquah MK, et al. An overview of immobilized enzyme technologies for dye and phenolic removal from wastewater. J Environ Chem Eng. 2019;7:102961.
2. Mirazizi F, Bahrami A, Soleimani Asl S, Zaribafan A, Haghbeen K, Aminzadeh S. Evaluation of oxidative enzymes for efficient oxidation of aniline and phenolic pollutants. Int J Environ Sci Te. 2018;15:1679–86.
3. Mohammadnejad P, Soleimani Asl S, Rasoulian Z, Aminzadeh S, Ghashghaie J, Haghbeen K. A potent peroxidase from solid cell culture of Ocimum basilicum with high sensitivity for blood glucose determination. Plant Cell Tiss Org. 2021;146:375–86.
4. Khan MR. Immobilized enzymes: a comprehensive review. Bull Natl Res Cent. 2021;45:207.
5. Valls-Chivas A, Gomez J, Garcia-Peiro JI, Hornos F, Hueso JL. Enzyme-iron oxide nanoassemblies: a review of immobilization and biocatalytic applications. Catalysts. 2023;13:980.
6. Slama HB, Chenari Bouket A, Pourhassan Z, Alenezi FN, Silini A, Cherif-Silini H, et al. Diversity of synthetic dyes from textile industries, discharge impacts and treatment methods. Appl Sci. 2021;11:6255.
7. Al-Tohamy R, Ali SS, Li F, Okasha KM, Mahmoud YAG, Elsamahy T, et al. A critical review on the treatment of dye-containing wastewater: Ecotoxicological and health concerns of textile dyes and possible remediation approaches for environmental safety. Ecotox Environ Safe. 2022;231:113160.
8. Kumar A, Ambade B, Sankar TK, Sethi SS, Kurwadkar S. Source identification and health risk assessment of atmospheric $PM_{2.5}$-bound polycyclic aromatic hydrocarbons in Jamshedpur, India. Sustain Cities Soc. 2020;52:101801.
9. Yaashikaa PR, Devi MK, Kumar PS. Advances in the application of immobilized enzyme for the remediation of hazardous pollutant: A review. Chemosphere. 2022;299:134390.
10. Shindhal T, Rakholiya P, Varjani S, Pandey A, Ngo HH, Guo W, et al. A critical review on advances in the practices and perspectives for the treatment of dye industry wastewater. Bioengineered. 2021;12:70–87.
11. Golbabaie M, Khosronejad A, Baharanchi AA, Marefatjoo MJ, Shahrjerdi A, Aminzadeh S, et al. Enzymatic remediation of water resources by a durable and potent peroxidase from the cell culture of *Origanum vulgare*. J Clean Prod. 2023;406:137126.
12. Haghbeen K, Tan EW. Facile Synthesis of catechol azo dyes. J Org Chem. 1998;63:4503–5.
13. Mohammadnejad P, Asl SS, Aminzadeh S, Haghbeen K. A new sensitive spectrophotometric method for determination of saliva and blood glucose. Spectrochim Acta A. 2020;229:117897.
14. Silva JMM, Feuser PE, Cercena R, Peterson M, Dal-Bo AG. Obtention of magnetite nanoparticles via the hydrothermal method and effect of synthesis parameters. J Magn Magn Mater. 2023;580:170925.
15. Natarajan S, Harini K, Gajula GP, Sarmento B, Neves-Petersen MT, Thiagarajan V. Multifunctional magnetic iron oxide nanoparticles: diverse synthetic approaches, surface modifications, cytotoxicity towards biomedical and industrial applications. BMC Mater. 2019;1:2.
16. Mizutani N, Iwasaki T, Watano S, Yanagida T, Tanaka H, Kawai T. Effect of ferrous/ferric ions molar ratio on reaction mechanism for hydrothermal synthesis of magnetite nanoparticles. B Mater Sci. 2008;31:713–7.
17. Haghbeen K, Legge RL. Adsorption of phenolic compounds on some hybrid xerogels. Chem Eng J. 2009;150:1–7.
18. Hassani S, Ghasemi A, Fazli M, Haghbeen K, Legge RL. Cation-assisted adsorption of chlorophenols by nano-xerogels. Can J Chem Eng. 2015;93:2214–21.
19. Cruz-Quesada G, Espinal-Viguri M, Lopez-Ramon MV, Garrido JJ. Novel silica hybrid xerogels prepared by co-condensation of TEOS and ClPhTEOS: A chemical and morphological study. Gels. 2022;8:677.
20. Abdollahi K, Yazdani F, Panahi R. Covalent immobilization of tyrosinase onto cyanuric chloride crosslinked amine-functionalized superparamagnetic nanoparticles: Synthesis and characterization of the recyclable nanobiocatalyst. Int J Biol Macromol. 2017;94:396–405.
21. Ho PY, Chiou MS, Chao AC. Production of l-DOPA by tyrosinase immobilized on modified polystyrene. Appl Biochem Biotech. 2003;111:139–52.
22. Sarimov RM, Nagaev EI, Matveyeva TA, Binhi VN, Burmistrov DE, Serov DA, et al. Investigation of aggregation and disaggregation of self-assembling nano-sized clusters consisting of individual iron oxide nanoparticles upon interaction with HEWL protein molecules. Nanomaterials. 2022;12:3960.
23. Almeida RM, Marques AC. Characterization of Sol-Gel Materials by Infrared Spectroscopy. In: Klein L, Aparicio M, Jitianu A, editors. Handbook of Sol-Gel Science and Technology. Cham: Springer International Publishing; 2016, p. 1–31.
24. Salem M, Mauguen Y, Prange T. Revisiting glutaraldehyde cross-linking: the case of the Arg-Lys intermolecular doublet. Acta Crystallogr F. 2010;66:225–8.
25. Hao A, Wang S, Huang J. Filling the pores of the post-cross-linked polymers with different rigid cross-linking bridges. ChemistrySelect. 2020;5:7941–6.
26. Foye WO, Buckpitt AE. Amine derivatives of cyanuric chloride. J Am Pharm Assoc Sci. 1952;41:385–7.
27. Fielder RJ, Bishop CT, Grappel SF, Blank F. An immunogenic polysaccharide-protein conjugate. J Immunol. 1970;105:265–7.
28. Padgett WM, II, Hamner WF. The infrared spectra of some derivatives of 1,3,5-triazine. J Am Chem Soc. 1958;80:803–8.
29. Just G, Pokorny I, Pritzkow W. Kinetic studies on the reaction of cyanuric chloride with amines. J Prak Chem-Chem Ztg. 1995;337:133–5.
30. Banjanac K, Mihailovic M, Prlainovic N, Stojanovic M, Carevic M, Marinkovic A, et al. Cyanuric chloride functionalized silica nanoparticles for covalent immobilization of lipase. J Chem Technol Biot. 2016;91:439–48.
31. Yotova L, Yaneva S, Marinkova D, Serfaty S. Co-immobilization of peroxidase and tyrosinase onto hybrid membranes obtained by the sol-gel method for the construction of an optical biosensor. Biotechnol Biotec Eq. 2013;27:3885–9.
32. De Meutter J, Goormaghtigh E. Evaluation of protein secondary structure from FTIR spectra improved after partial deuteration. Eur Biophys J. 2021;50:613–28.
33. Azizi T, De Araujo LC, Cetecioglu Z, Clancy AJ, Feger ML, Liran O, et al. A COST Action on microbial responses to low pH: Developing links and sharing resources across the academic-industrial divide. New Biotechnol. 2022;72:64–70.
34. Soleimani Asl S, Karkhane AA, Zamani Amirzakaria J, Akbari Noghabi K, Ghashghaie J, haghbeen K. Structure and activity of a novel robust peroxidase from *Alkanna frigida* cell culture. Phytochemistry. 2022;194:113022.
35. Jun LY, Mubarak NM, Yon LS, Bing CH, Khalid M, Jagadish P, et al. Immobilization of peroxidase on functionalized MWCNTs-buckypaper/polyvinyl alcohol nanocomposite membrane. Sci Rep-Uk. 2019;9:2215.
36. Akpınar F, Evli S, Guven G, Bayraktaroglu M, Kilimci U, Uygun M, et al. Peroxidase immobilized cryogels for phenolic compounds removal. Appl Biochem Biotech. 2020;190:138–47.
37. Job D, Dunford HB. Substituent effect on the oxidation of phenols and aromatic amines by horseradish peroxidase compound I. Eur J Biochem. 1976;66:607–14.
38. Alikhani N, Shahedi M, Habibi Z, Yousefi M, Ghasemi S, Mohammadi M. A multi-component approach for co-immobilization of lipases on silica-coated magnetic nanoparticles: improving biodiesel production from waste cooking oil. Bioproc Biosyst Eng. 2022;45:2043–60.
39. de Andrade Silva T, Keijok WJ, Guimaraes MCC, Cassini STA, de Oliveira JP. Impact of immobilization strategies on the activity and recyclability of lipases in nanomagnetic supports. Sci Rep-Uk. 2022;12:6815.

Publisher's Note